BLACK HOLES

Polarized x-rays constrain the disk-jet geometry in the black hole x-ray binary Cygnus X-1

Henric Krawczynski[1]*, Fabio Muleri[2]*, Michal Dovčiak[3]*, Alexandra Veledina[4,5,6]*, Nicole Rodriguez Cavero[1], Jiri Svoboda[3], Adam Ingram[7], Giorgio Matt[8], Javier A. Garcia[9], Vladislav Loktev[4], Michela Negro[10,11,12], Juri Poutanen[4,6], Takao Kitaguchi[13], Jakub Podgorný[3,14,15], John Rankin[2], Wenda Zhang[16], Andrei Berdyugin[4], Svetlana V. Berdyugina[17,18,19], Stefano Bianchi[8], Dmitry Blinov[20,21], Fiamma Capitanio[2], Niccolò Di Lalla[22], Paul Draghis[23], Sergio Fabiani[2], Masato Kagitani[24], Vadim Kravtsov[4], Sebastian Kiehlmann[20,21], Luca Latronico[25], Alexander A. Lutovinov[6], Nikos Mandarakas[20,21], Frédéric Marin[14], Andrea Marinucci[26], Jon M. Miller[23], Tsunefumi Mizuno[27], Sergey V. Molkov[6], Nicola Omodei[22], Pierre-Olivier Petrucci[28], Ajay Ratheesh[2], Takeshi Sakanoi[24], Andrei N. Semena[6], Raphael Skalidis[20,21], Paolo Soffitta[2], Allyn F. Tennant[29], Phillipp Thalhammer[30], Francesco Tombesi[31,32,33], Martin C. Weisskopf[29], Joern Wilms[30], Sixuan Zhang[27], Iván Agudo[34], Lucio A. Antonelli[35,36], Matteo Bachetti[37], Luca Baldini[38,39], Wayne H. Baumgartner[29], Ronaldo Bellazzini[38], Stephen D. Bongiorno[29], Raffaella Bonino[25,40], Alessandro Brez[38], Niccolò Bucciantini[41,42,43], Simone Castellano[38], Elisabetta Cavazzuti[26], Stefano Ciprini[32,36], Enrico Costa[2], Alessandra De Rosa[2], Ettore Del Monte[2], Laura Di Gesu[26], Alessandro Di Marco[2], Immacolata Donnarumma[26], Victor Doroshenko[44,6], Steven R. Ehlert[29], Teruaki Enoto[13], Yuri Evangelista[2], Riccardo Ferrazzoli[2], Shuichi Gunji[45], Kiyoshi Hayashida[46]†, Jeremy Heyl[47], Wataru Iwakiri[48], Svetlana G. Jorstad[49,50], Vladimir Karas[3], Jeffery J. Kolodziejczak[29], Fabio La Monaca[2], Ioannis Liodakis[51], Simone Maldera[25], Alberto Manfreda[38], Alan P. Marscher[49], Herman L. Marshall[52], Ikuyuki Mitsuishi[53], Chi-Yung Ng[54], Stephen L. O'Dell[29], Chiara Oppedisano[25], Alessandro Papitto[35], George G. Pavlov[55], Abel L. Peirson[22], Matteo Perri[36,35], Melissa Pesce-Rollins[38], Maura Pilia[37], Andrea Possenti[37], Simonetta Puccetti[36], Brian D. Ramsey[29], Roger W. Romani[22], Carmelo Sgrò[38], Patrick Slane[56], Gloria Spandre[38], Toru Tamagawa[15], Fabrizio Tavecchio[57], Roberto Taverna[58], Yuzuru Tawara[53], Nicholas E. Thomas[29], Alessio Trois[37], Sergey Tsygankov[4,6], Roberto Turolla[58,59], Jacco Vink[60], Kinwah Wu[59], Fei Xie[2,61], Silvia Zane[59]

A black hole x-ray binary (XRB) system forms when gas is stripped from a normal star and accretes onto a black hole, which heats the gas sufficiently to emit x-rays. We report a polarimetric observation of the XRB Cygnus X-1 using the Imaging X-ray Polarimetry Explorer. The electric field position angle aligns with the outflowing jet, indicating that the jet is launched from the inner x-ray–emitting region. The polarization degree is 4.01 ± 0.20% at 2 to 8 kiloelectronvolts, implying that the accretion disk is viewed closer to edge-on than the binary orbit. These observations reveal that hot x-ray–emitting plasma is spatially extended in a plane perpendicular to, not parallel to, the jet axis.

Cygnus X-1 (Cyg X-1, also cataloged as HD 226868) is a bright and persistent x-ray source. It is a binary system containing a 21.2 ± 2.2 solar-mass black hole in a 5.6-day orbit with a $40.6^{+7.7}_{-7.1}$ solar-mass star and is located at a distance of $2.22^{+0.18}_{-0.17}$ kiloparsecs (kpc) (*1*). Gas is stripped from the companion star; as it falls in the strong gravitational field of the black hole, it forms an accretion disk that is heated to millions of kelvin. The hot incandescent gas emits x-rays. Previous analyses of the thermal x-ray flux, its energy spectrum, and the shape of the x-ray emission lines have indicated that the black hole in Cyg X-1 spins rapidly, with a dimensionless spin parameter $a > 0.92$ (close to the maximum possible value of 1) (*2*). Cyg X-1 also produces two pencil-shaped outflows of magnetized plasma, called jets, that have been imaged in the radio band (*3*). It is therefore classified as a microquasar, being analogous to much larger radio-loud quasars (supermassive black holes with jets).

Black hole x-ray binaries are observed in states of x-ray emission thought to correspond to different configurations of the accreting matter (*4*). In the soft state, the x-rays are dominated by thermal emission from the accretion disk. The thermal emission is expected to be polarized because x-rays scatter off electrons in the accretion disk (*5*–*7*). In the hard state, the x-ray emission is produced by (single or multiple) scattering of photons (emitted by the accretion disk or electrons in the magnetic field) off electrons in hot coronal gas. Observations constrain the corona to be much hotter ($k_B T_e \sim 100$ keV, where k_B is the Boltzmann constant and T_e is the electron temperature) than the accretion disk ($k_B T_d \sim 0.1$ keV, where T_d is the disk temperature). The shape of the corona and its location with respect to the accretion disk are both debated (*4*, *8*) but could be constrained by x-ray polarimetry (*9*). Reflection of x-rays emitted by the corona off the accretion disk produces an emission component that includes the iron Kα fluorescence line at ~6.4 keV, which can constrain the velocity of the accretion disk gas orbiting the black hole and the time dilation close to the black hole. This reflection component is also expected to be polarized (*10*, *11*).

We performed x-ray polarimetric observations of Cyg X-1 using the Imaging X-ray Polarimetry Explorer (IXPE) space telescope (*12*). Theoretical predictions of the Cyg X-1 polarization degree (in the 2–8 keV IXPE band) were ~1% or lower, depending on the emission state (*6*, *7*, *9*, *13*). These predictions used an inclination angle (the angle between the black hole spin axis and the line of sight) of $i = 27.^{\circ}5 \pm 0.^{\circ}8$ inferred from optical observations of the binary system (*1*). Earlier polarization observations with the Eighth Orbiting Solar Observatory (OSO-8) space telescope gave a polarization degree of 2.44 ± 1.07% and a polarization angle (measured on the plane of the sky from north to east) of −18° ± 13° at 2.6 keV (*14*, *15*) and a nondetection at higher energies (*16*). IXPE observed Cyg X-1 from 15 to 21 May 2022 with an exposure time of ~242 kiloseconds (ks). The IXPE 2–8 keV observations were coordinated with simultaneous x-ray and gamma-ray observations by other space telescopes covering the energy range 0.2–250 keV, including the Neutron Star Interior Composition Explorer (NICER, 0.2–12 keV), the Nuclear Spectroscopic Telescope Array (NuSTAR, 3–79 keV), the Swift X-ray Telescope (XRT, 0.2–10 keV), the Astronomical Roentgen Telescope–X-ray Concentrator (ART-XC, 4–30 keV) of the Spectrum-Röntgen-Gamma observatory (SRG), and the INTEGRAL Soft Gamma-Ray Imager (ISGRI, 30–80 keV) on the International Gamma-Ray Astrophysics Laboratory (INTEGRAL) (*17*). Simultaneous optical observations were performed with the Double Image Polarimeter 2 (DIPol-2) instrument mounted on the Tohoku 60-cm telescope at the Haleakala Observatory, Hawaii, and the Robotic Polarimeter (RoboPol) at the 1.3-m telescope of the Skinakas Observatory, Greece (*17*).

During the observation campaign, Cyg X-1 was highly variable over the entire 0.2–250 keV energy range (fig. S1). The source was in the hard x-ray state with a photon index of 1.6 (table S5) and a 0.2–250 keV luminosity of 1.1% of the Eddington luminosity (the luminosity at which the radiation pressure on electrons equals the gravitational pull on the ions of the accreted material). We detected linear polarization in the IXPE data with >20σ statistical confidence (where σ is the standard deviation) (Fig. 1 and fig. S3), measuring a 2–8 keV polarization degree of 4.01 ± 0.20% at an electric field position angle of $-20.^{\circ}7 \pm 1.^{\circ}4$. The polarization degree and angle are consistent with the previous results of OSO-8 at 2.6 keV (*15*). Evidence for an increase in the polarization degree with energy

(Fig. 1 and fig. S5) is significant at the 3.4σ level (*17*). We find a 2.4σ indication that the polarization degree increases with the source flux (fig. S6).

We find no evidence that the polarization depends on the orbital phase of the binary system (fig. S7). This excludes the possibility that the observed x-ray polarization originates from the scattering of x-ray photons off the companion star or its wind and shows that these effects do not measurably affect the polarization properties.

We calculated a suite of emission models and compared them with the observations (*17*). We estimate that >90% of the x-rays come from the inner ~2000-km-diameter region surrounding the ~60-km-diameter black hole. The x-ray polarization angle aligns with the billion-kilometer-scale radio jet to within ~5° (Fig. 2).

We decomposed the broadband energy spectra observed simultaneously with IXPE, NICER, NuSTAR, and INTEGRAL into a multi-temperature black-body component (thermal emission from the accretion disk), a power-law component (from multiple Compton scattering events in the corona), emission reflected off the accretion disk, and emission from more distant stationary plasma (fig. S8) (*17*). We find that the coronal emission strongly dominates in the IXPE energy band, contributing ~90% of the observed flux. The accretion disk and reflected emission components contribute <1% and ~10% of the emission, respectively. Therefore, our polarization measurements are likely to be dominated by the coronal emission.

We analyzed the optical data at multiple wavelengths (*17*), finding an intrinsic optical polarization degree of ~1% and polarization angle of –24°. The uncertainties on these results are dominated by systematic effects related to the choice of polarization reference stars and are ±0.1% on the polarization degree and ±13° on the polarization direction (figs. S11 to S13 and table S4). The optical polarization direction is thought to indicate the orientation of the orbital axis projected onto the sky (*18*). We find that it aligns with the x-ray polarization direction and the radio jet.

The alignment of the x-ray polarization with the radio jet indicates that the inner x-ray–emitting region is directly related to the radio jet. If the x-ray polarization is perpendicular to the inner accretion disk plane, as favored in our models (*17*), this implies that the inner accretion disk is perpendicular to the radio jet, at least on the plane of the sky. This is consistent with the hypothesis that jets of microquasars (and, by extension, of quasars) are launched perpendicular to the inner accretion flow (*19*).

Figure 3 compares our observed polarization with theoretical predictions made using models of the corona (*17*). We find that the only models that are consistent with the observations are those in which the coronal plasma is extended perpendicular to the jet axis, and therefore probably parallel to the accretion disk. In these models, repeated scatterings in the plane of the corona polarize the x-rays perpendicular to that plane. Two models are consistent with our observations: (i) a hot corona sandwiching the accretion disk (*20*), as predicted by numerical accretion disk simulations (*21*); or (ii) a composite accretion flow with a truncated cold disk that is geometrically thin and optically thick and an inner laterally extended region (geometrically thick but optically thin) of hot plasma, possibly produced by evaporation of the cold disk (*22*). If the jet is launched from the inner, magnetized region of the disk, the jet carrying away disk angular momentum could leave behind a radially extended hot and optically thin corona (*23*).

The polarization data rule out models in which the corona is a narrow plasma column or cone along the jet axis, or consists of two compact regions above and below the black hole. Our modeling of these scenarios accounts for the effect of the coronal emission reflecting off the accretion disk (*17*). These models predict polarization degree well below the observed values. Models that produce high polarization degree predict polarization directions close to perpendicular to the jet axis, a decreasing polarization degree with energy, or both, and therefore disagree with the observations.

In our favored corona models, the high polarization degree we observe requires that the x-ray bright region is seen at a higher inclination than the ~27° inclination of the binary orbit. Sandwich corona models involving the

[1]Department of Physics and McDonnell Center for the Space Sciences, Washington University in St. Louis, St. Louis, MO 63130, USA. [2]Istituto di Astrofisica e Planetologia Spaziali, Istituto Nazionale di Astrofisica (INAF), 00133 Roma, Italy. [3]Astronomical Institute of the Czech Academy of Sciences, 14100 Praha 4, Czech Republic. [4]Department of Physics and Astronomy, 20014 University of Turku, Turku, Finland. [5]Nordic Institute for Theoretical Physics (Nordita), Kungliga Tekniska Högskolan (KTH) Royal Institute of Technology and Stockholm University, SE-106 91 Stockholm, Sweden. [6]Space Research Institute of the Russian Academy of Sciences, Moscow 117997, Russia. [7]School of Mathematics, Statistics, and Physics, Newcastle University, Newcastle upon Tyne NE1 7RU, UK. [8]Dipartimento di Matematica e Fisica, Università degli Studi Roma Tre, 00146 Roma, Italy. [9]Division of Physics, Mathematics and Astronomy, California Institute of Technology, Pasadena, CA 91125, USA. [10]Center for Space Sciences and Technology, University of Maryland, Baltimore County, Baltimore, MD 21250, USA. [11]NASA Goddard Space Flight Center (GSFC), Greenbelt, MD 20771, USA. [12]Center for Research and Exploration in Space Science and Technology, NASA-GSFC, Greenbelt, MD 20771, USA. [13]Rikagaku Kenkyūjyo (RIKEN) Cluster for Pioneering Research, 2-1 Hirosawa, Wako, Saitama 351-0198, Japan. [14]Centre national de la recherche scientifique, Observatoire Astronomique de Strasbourg, Université de Strasbourg, Unité Mixte de Recherche 7550, 67000 Strasbourg, France. [15]Astronomical Institute, Charles University, 18000 Prague, Czech Republic. [16]National Astronomical Observatories, Chinese Academy of Sciences, Beijing 100101, China. [17]Leibniz-Institut für Sonnenphysik, 79104 Freiburg, Germany. [18]Istituto Ricerche Solari (IRSOL) Aldo e Cele Daccò, Faculty of Informatics, Università della Svizzera italiana, 6605 Locarno, Switzerland. [19]Euler Institute, Faculty of Informatics, Università della Svizzera italiana, 6962 Lugano, Switzerland. [20]Institute of Astrophysics, Foundation for Research and Technology–Hellas, 71110 Heraklion, Greece. [21]Department of Physics, University of Crete, 70013 Heraklion, Greece. [22]Department of Physics and Kavli Institute for Particle Astrophysics and Cosmology, Stanford University, Stanford, CA 94305, USA. [23]Department of Astronomy, University of Michigan, Ann Arbor, MI 48109, USA. [24]School of Sciences, Tohoku University, Aoba-ku, 980-8578 Sendai, Japan. [25]Istituto Nazionale di Fisica Nucleare, Sezione di Torino, 10125 Torino, Italy. [26]Agenzia Spaziale Italiana (ASI), 00133 Roma, Italy. [27]Hiroshima Astrophysical Science Center, Hiroshima University, 1-3-1 Kagamiyama, Higashi-Hiroshima, Hiroshima 739-8526, Japan. [28]Institut de Planétologie et d'Astrophysique de Grenoble (IPAG), Université Grenoble Alpes, Centre national de la recherche scientifique, 38000 Grenoble, France. [29]NASA Marshall Space Flight Center, Huntsville, AL 35812, USA. [30]Dr. Karl Remeis Observatory, Erlangen Centre for Astroparticle Physics, Universität Erlangen-Nürnberg, 96049 Bamberg, Germany. [31]Dipartimento di Fisica, Università degli Studi di Roma "Tor Vergata," 00133 Roma, Italy. [32]Istituto Nazionale di Fisica Nucleare, Sezione di Roma "Tor Vergata," 00133 Roma, Italy. [33]Department of Astronomy, University of Maryland, College Park, MD 20742, USA. [34]Instituto de Astrofísica de Andalucía, 18008 Granada, Spain. [35]INAF Osservatorio Astronomico di Roma, 00078 Monte Porzio Catone, Roma, Italy. [36]Space Science Data Center, ASI, 00133 Roma, Italy. [37]INAF Osservatorio Astronomico di Cagliari, 09047 Selargius, Cagliari, Italy. [38]Istituto Nazionale di Fisica Nucleare, Sezione di Pisa, 56127 Pisa, Italy. [39]Dipartimento di Fisica, Università di Pisa, 56127 Pisa, Italy. [40]Dipartimento di Fisica, Università degli Studi di Torino, 10125 Torino, Italy. [41]INAF Osservatorio Astrofisico di Arcetri, 50125 Firenze, Italy. [42]Dipartimento di Fisica e Astronomia, Università degli Studi di Firenze, 50019 Sesto Fiorentino, Firenze, Italy. [43]Istituto Nazionale di Fisica Nucleare, Sezione di Firenze, 50019 Sesto Fiorentino, Firenze, Italy. [44]Institut für Astronomie und Astrophysik, Universität Tübingen, 72076 Tübingen, Germany. [45]Department of Physics, Yamagata University, 1-4-12 Kojirakawa-machi, Yamagata-shi 990-8560, Japan. [46]Department of Earth and Space Science, Osaka University, 1-1 Yamadaoka, Suita, Osaka 565-0871, Japan. [47]Department of Physics and Astronomy, University of British Columbia, Vancouver, BC V6T 1Z4, Canada. [48]Department of Physics, Faculty of Science and Engineering, Chuo University, 1-13-27 Kasuga, Bunkyo-ku, Tokyo 112-8551, Japan. [49]Institute for Astrophysical Research, Boston University, Boston, MA 02215, USA. [50]Department of Astrophysics, St. Petersburg State University, Petrodvoretz, 198504 St. Petersburg, Russia. [51]Finnish Centre for Astronomy with the European Southern Observatory (ESO), 20014 University of Turku, Turku, Finland. [52]Kavli Institute for Astrophysics and Space Research, Massachusetts Institute of Technology, Cambridge, MA 02139, USA. [53]Division of Particle and Astrophysical Science, Graduate School of Science, Nagoya University, Furo-cho, Chikusa-ku, Nagoya, Aichi 464-8602, Japan. [54]Department of Physics, The University of Hong Kong, Pokfulam, Hong Kong. [55]Department of Astronomy and Astrophysics, Pennsylvania State University, University Park, PA 16802, USA. [56]Center for Astrophysics, Harvard & Smithsonian, Cambridge, MA 02138, USA. [57]INAF Osservatorio Astronomico di Brera, 23807 Merate, Lecco, Italy. [58]Dipartimento di Fisica e Astronomia, Università degli Studi di Padova, 35131 Padova, Italy. [59]Mullard Space Science Laboratory, University College London, Holmbury St Mary, Dorking, Surrey RH5 6NT, UK. [60]Anton Pannekoek Institute for Astronomy, University of Amsterdam, 1098 XH Amsterdam, Netherlands. [61]Guangxi Key Laboratory for Relativistic Astrophysics, School of Physical Science and Technology, Guangxi University, Nanning 530004, China.

***Corresponding author. Email: krawcz@wustl.edu (H.K.); fabio.muleri@inaf.it (F.Mu.); dovciak@astro.cas.cz (M.D.); alexandra.veledina@utu.fi (A.V.)**

†Deceased.

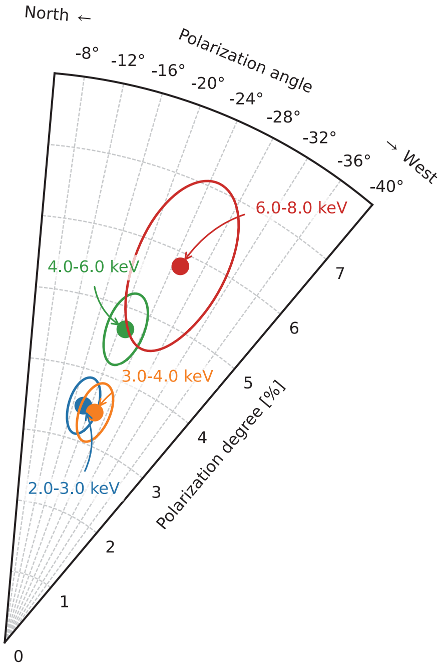

Fig. 1. Energy-dependent x-ray polarization of Cyg X-1. The polarization degree and polarization angle, derived from the IXPE observations, are shown for four energy bands (labeled and in different colors). The ellipses denote the 68.3% confidence regions.

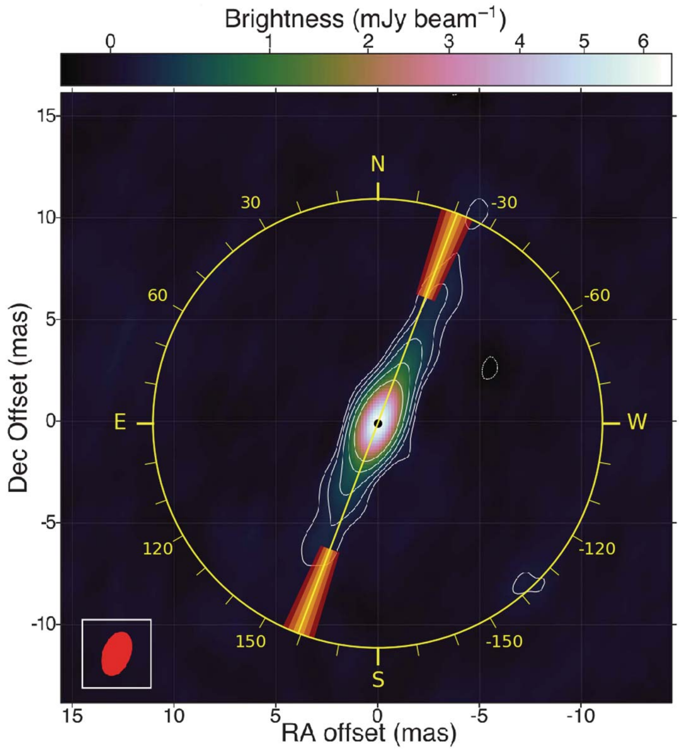

Fig. 2. Comparison of the x-ray polarization direction with the radio jet. The 2–8 keV electric vector position angle is shown with the yellow line, and the 1σ, 2σ, and 3σ confidence regions are given by the orange-to-red shading. The background image is a radio observation of the jet (*1*). We infer (see text) that most x-rays are emitted by a ~2000-km-diameter region surrounding the ~60-km-diameter black hole, far smaller than the resolution of the radio image (which is indicated by the red ellipse). The coordinate offsets in right ascension (RA) and declination (Dec) (J2000 equinox) are in units of milliarcseconds (mas). The color scale shows the radio flux in milli-Jansky, with 1 Jansky being 10^{-26} W m^{-2} Hz^{-1}.

Compton scattering of disk photons with initial energies of ~0.1 keV require inclinations exceeding 65°. Truncated disk models invoking Compton scattering of the disk or internally generated lower-energy (~1–10 eV) synchrotron photons (*24*) can reproduce the observed polarization degree for inclinations of >45°. In comparison to the models with disk photons, the larger number of scatterings required to energize lower-energy synchrotron photons to kiloelectronvolt energies results in higher polarization degree in the IXPE energy band (fig. S9) (*17*).

Although the x-ray polarization, optical polarization, and radio jet approximately align in the plane of the sky, the inclination of the x-ray bright region exceeds that of the binary orbit, implying that the inner accretion flow is seen more edge-on than the binary orbit. Because the bodies of a stellar system typically orbit and spin around the same axis (as do most planets in the Solar System), we consider potential explanations for the mismatch between the inner accretion disk inclination and the orbital inclination.

Stellar-mass black holes are formed during supernovae. The supernova that occurred in Cyg X-1 might have left the black hole with a misaligned spin. Gravitational effects could align the inner accretion flow angular momentum vector with the black hole spin vector (*25*). In this scenario, aligning the inner accretion disk angular momentum vector with the black hole spin vector would also align the radio jet produced by the inner accretion disk with the black hole spin vector. Several, but not all, analyses of Cyg X-1 reflected emission spectra give inclinations consistent with our $i > 45°$ constraint (*26*, *27*).

An alternative explanation for the large inclination of the x-ray–emitting region invokes the precession of the inner accretion flow with a period much longer than the orbital period (*28*). From our analysis of a 2–4 keV long-term x-ray light curve, we infer that the IXPE observations were performed close to the maximum inner disk inclination (fig. S2) (*17*). We tested the hypothesis that the inner flow precesses with an amplitude of ≳17°.5 by performing an additional 86-ks IXPE target of opportunity observation of Cyg X-1 from 18 to 20 June 2022, 33 days after the May observations, which corresponds to half of the current superorbital period (*17*). If this hypothesis is correct, we expect the polarization degree to drop from 4.01 ± 0.20% to ≪1% owing to the inclination changing from $i > 45°$ in May to $i \lesssim 10°$ in June. The observations showed the source in the same hard state with a 2–8 keV polarization degree and angle of 3.84 ± 0.31% and −25°.7 ± 2°.3, respectively (fig. S4) (*17*). The polarization degree remained constant (within the statistical uncertainties) between the May and June observations. We therefore disfavor the hypothesis that precession of the inner accretion flow leads to the high polarization degree of the May observation. The combined May and June polarization degree and angle are 3.95 ± 0.17% and −22.°2 ± 1°.2, respectively (fig. S4) (*17*).

In previous work, others have argued that optically thin synchrotron emission from the base of the jet could contribute up to 5% to the Cyg X-1 x-ray emission in the hard state (*29*, *30*). Synchrotron emission from electrons gyrating around magnetic field lines is polarized perpendicular to those field lines. Our observation of the x-rays being polarized parallel to the jet axis would require synchrotron emission from a toroidal magnetic field, wound around the jet axis. For this magnetic field geometry, seen at an inclination of 27°.5, the theoretical upper limit on the polarization degree of the synchrotron emission is 8% (*31*). The jet thus contributes <0.4% of the observed polarization degree. If the almost-constant jet

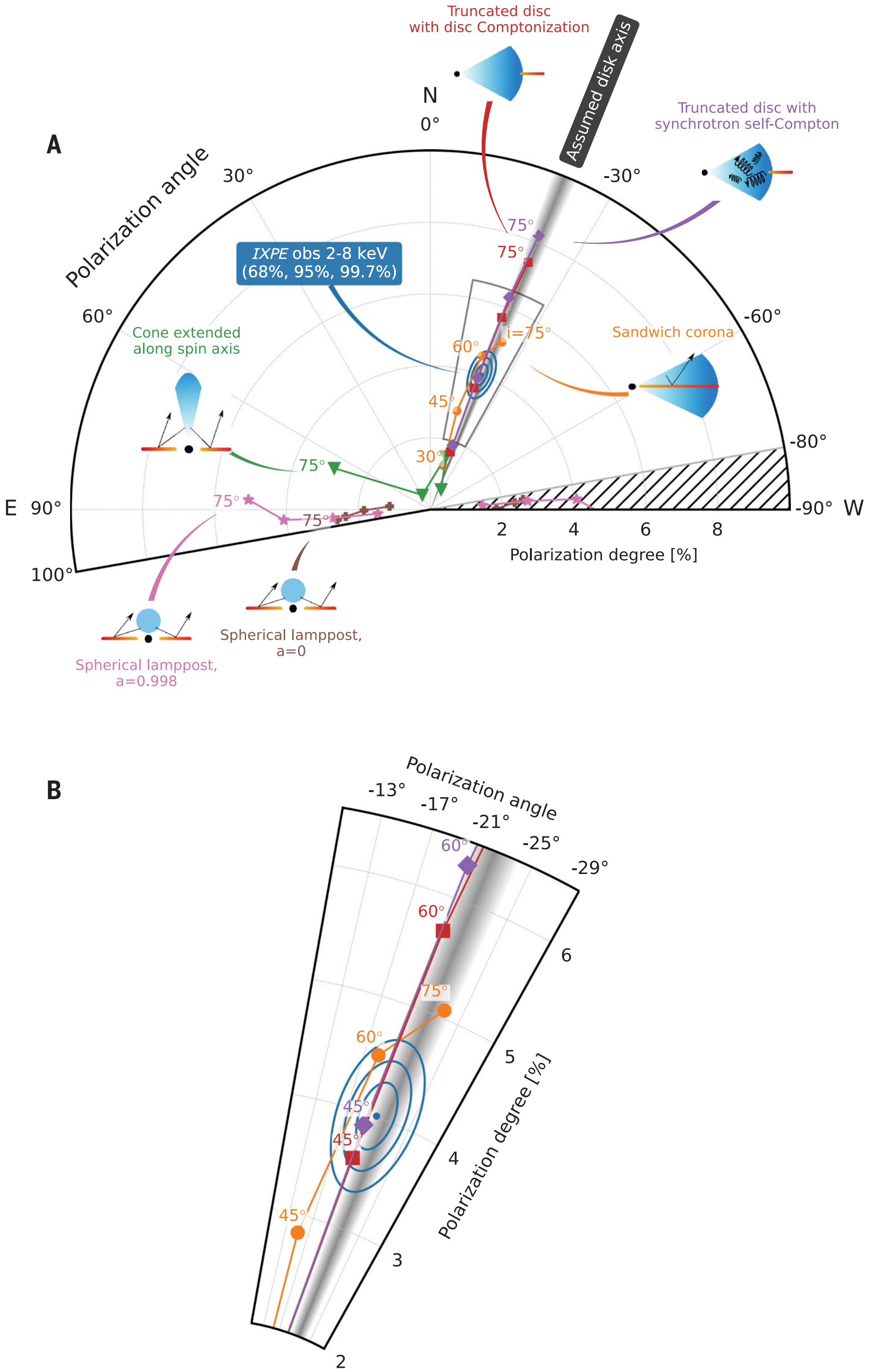

Fig. 3. Comparison of the observed 2–8 keV polarization degree and angle with model predictions. (**A**) The blue dot shows the polarization degree and angle, with the blue ellipses indicating the 68, 95, and 99.7% confidence levels (equivalent to 1σ, 2σ, and 3σ, respectively). Model predictions assume that the inner disk spin axis has position angle of −22° (consistent with the radio jet), and that the inner disk angular momentum vector points away from the observer (as does the orbital angular momentum vector) (*1*). The gray band shows the uncertainty of the radio jet orientation; we adopt this as the uncertainty of the disk spin axis in all models. Each colored line shows the model results for each chosen corona geometry, with symbols indicating different values as a function of the inner disk inclination *i*. Inset diagrams schematically depict the assumed black hole (black), corona (blue), and accretion disk (orange-red) configurations. Black arrows indicate photon paths. Models with coronae extending parallel to the inner accretion disk can match the IXPE observations, but coronae located or extending along the spin axis of the inner accretion disk cannot. The position angles are shown from −80° to +100° (instead of −90° to +90°) to clarify the models that straddle the ±90° borders. (**B**) A zoom into the region around the measured value, marked with the gray box in (A).

emission was the main source of the observed polarization, we would expect that a rise in the x-ray flux from the inner accretion flow would lead to an overall smaller polarization degree—contrary to the observed trend (fig. S6).

The polarized x-rays from the immediate surroundings of the black hole carry the imprint of the geometry of the emitting gas. We conclude that the x-ray bright plasma is extended perpendicular to the radio jet. The high observed polarization degree either implies a more edge-on viewing geometry than given by the optical data, or it suggests that unidentified physical effects are responsible for production of the x-rays in accreting black hole systems.

REFERENCES AND NOTES

1. J. C. A. Miller-Jones *et al.*, *Science* **371**, 1046–1049 (2021).
2. L. Gou *et al.*, *Astrophys. J.* **790**, 29 (2014).
3. A. M. Stirling *et al.*, *Mon. Not. R. Astron. Soc.* **327**, 1273–1278 (2001).
4. C. Done, M. Gierliński, A. Kubota, *Astron. Astrophys. Rev.* **15**, 1–66 (2007).
5. P. A. Connors, T. Piran, R. F. Stark, *Astrophys. J.* **235**, 224 (1980).
6. L.-X. Li, R. Narayan, J. E. McClintock, *Astrophys. J.* **691**, 847–865 (2009).
7. J. D. Schnittman, J. H. Krolik, *Astrophys. J.* **701**, 1175–1187 (2009).
8. C. Bambi *et al.*, *Space Sci. Rev.* **217**, 65 (2021).
9. J. D. Schnittman, J. H. Krolik, *Astrophys. J.* **712**, 908–924 (2010).

10. G. Matt, *Mon. Not. R. Astron. Soc.* **260**, 663–674 (1993).
11. J. Poutanen, K. N. Nagendra, R. Svensson, *Mon. Not. R. Astron. Soc.* **283**, 892–904 (1996).
12. M. C. Weisskopf *et al*., *J. Astron. Telesc. Instrum. Syst.* **8**, 026002 (2022).
13. H. Krawczynski, B. Beheshtipour, *Astrophys. J.* **934**, 4 (2022).
14. M. C. Weisskopf *et al*., *Astrophys. J.* **215**, L65 (1977).
15. K. S. Long, G. A. Chanan, R. Novick, *Astrophys. J.* **238**, 710 (1980).
16. M. Chauvin *et al*., *Nat. Astron.* **2**, 652–655 (2018).
17. Materials and methods are available as supplementary materials.
18. J. C. Kemp, M. S. Barbour, T. E. Parker, L. C. Herman, *Astrophys. J.* **228**, L23–L27 (1979).
19. M. C. Begelman, R. D. Blandford, M. J. Rees, *Rev. Mod. Phys.* **56**, 255–351 (1984).
20. F. Haardt, L. Maraschi, *Astrophys. J.* **380**, L51 (1991).
21. B. E. Kinch, J. D. Schnittman, S. C. Noble, T. R. Kallman, J. H. Krolik, *Astrophys. J.* **922**, 270 (2021).
22. F. Meyer, E. Meyer-Hofmeister, *Astron. Astrophys.* **288**, 175–182 (1994).
23. P. O. Petrucci, J. Ferreira, G. Henri, J. Malzac, C. Foellmi, *Astron. Astrophys.* **522**, A38 (2010).
24. A. Veledina, J. Poutanen, I. Vurm, *Mon. Not. R. Astron. Soc.* **430**, 3196–3212 (2013).
25. J. M. Bardeen, J. A. Petterson, *Astrophys. J.* **195**, L65 (1975).
26. J. A. Tomsick *et al*., *Astrophys. J.* **780**, 78 (2014).
27. M. L. Parker *et al*., *Astrophys. J.* **808**, 9 (2015).
28. P. Lachowicz, A. A. Zdziarski, A. Schwarzenberg-Czerny, G. G. Pooley, S. Kitamoto, *Mon. Not. R. Astron. Soc.* **368**, 1025–1039 (2006).
29. D. M. Russell, T. Shahbaz, *Mon. Not. R. Astron. Soc.* **438**, 2083–2096 (2014).
30. A. A. Zdziarski, P. Pjanka, M. Sikora, Ł. Stawarz, *Mon. Not. R. Astron. Soc.* **442**, 3243–3255 (2014).
31. M. Lyutikov, V. I. Pariev, D. C. Gabuzda, *Mon. Not. R. Astron. Soc.* **360**, 869–891 (2005).
32. P. Thalhammer, J. Wilms, N. Rodriguez Cavero, X-ray observations of black hole binary Cyg X-1 with INTEGRAL, version 1, Zenodo (2022); https://doi.org/10.5281/zenodo.7140274.
33. V. Kravtsov *et al*., Optical polarimetric observations of black hole binary Cyg X-1 with DIPol-2, version 1, Zenodo (2022); https://doi.org/10.5281/zenodo.7108247.
34. D. Blinov, S. Kiehlmann, N. Mandarakas, R. Skalidis, Optical polarimetric observations of the black hole binary star Cyg X-1 with RoboPol, version 1, Zenodo (2022); https://doi.org/10.5281/zenodo.7127802.
35. W. Zhang, M. Dovčiak, M. Bursa, *Astrophys. J.* **875**, 148 (2019).
36. A. Veledina, J. Poutanen, Polarization of Comptonized emission in slab geometry, version 1, Zenodo (2022); https://doi.org/10.5281/zenodo.7116125.

ACKNOWLEDGMENTS

We thank J. Miller-Jones, J. Orosz, and A. Zdziarski for very helpful discussions of the optical constraints on the orbital inclination of Cyg X-1 and optical position angles. We are grateful to three anonymous referees, whose excellent comments contributed to strengthening the paper. We thank T. Maccarone for emphasizing that stellar wind absorption may modify the jet orientation measurement results. This work is based on observations made with the IXPE mission, a joint US and Italian mission. The US contribution to the IXPE mission is supported by NASA and led and managed by its Marshall Space Flight Center, with industry partner Ball Aerospace (contract NNM15AA18C). The Italian contribution to the IXPE mission is supported by the Italian Space Agency (ASI) through contract ASI-OHBI-2017-12-I.0, agreements ASI-INAF-2017-12-H0 and ASI-INFN-2017.13-H0, and its Space Science Data Center (SSDC) with agreements ASI-INAF-2022-14-HH.0 and ASI-INFN 2021-43-HH.0; and by INAF and the Istituto Nazionale di Fisica Nucleare (INFN) in Italy. This research used data and software products or online services provided by the IXPE Team (Marshall Space Flight Center, the SSDC of the Italian Space Agency, the INAF, and INFN), as well as the High-Energy Astrophysics Science Archive Research Center (HEASARC), at NASA Goddard Space Flight Center. We thank the NICER, NuSTAR, INTEGRAL, Swift, and SRG/ART-XC teams and Science Operation Centers for their support of this observation campaign. DIPol-2 is a joint effort between University of Turku (Finland) and Leibniz Institut für Sonnenphysik (Germany). We are grateful to the Institute for Astronomy, University of Hawaii, for allocating observing time for the DIPol-2 polarimeter, and to the Skinakas Observatory for performing the observations with the RoboPol polarimeter at their 1.3-m telescope. **Funding:** H.K. acknowledges NASA support under grants 80NSSC18K0264, 80NSSC22K1291, 80NSSC21K1817, and NNX16AC42G. F.Mu., J.R., S.B., S.F., A.R., P.So., E.D.M., E.Co., A.D.M., G.M., Y.E., R.F., F.L.M., M.Pe., and A.T. were funded through contract ASI-INAF-2017-12-H0. L.B., R.Bo., R.Be., A.Br., L.L., S.Ca., S.M., A.Man., C.O., M.P.-R., C.S., and G.S. were funded by the ASI through contracts ASI-INFN-2017.13-H0 and ASI-INFN 2021-43-HH.0. M.Pi. was funded through contract ASI-INAF-2022-14-HH.0. I.A. acknowledges support from MICINN (Ministerio de Ciencia e Innovación) Severo Ochoa award for the IAA-CSIC (SEV-2017-0709) and through grants AYA2016-80889-P and PID2019-107847RB-C44. M.D., J.S., and V.Ka. acknowledge support from GACR (Grantová agentura České republiky) project 21-06825X and institutional support from the Astronomical Institute of the Czech Academy of Sciences (RVO:67985815). J.A.G. acknowledges support from NASA grant 80NSSC20K0540. J.Pod. acknowledges support from Charles University project GA UK No. 174121 and from the Barrande Fellowship Programme of the Czech and French governments. A.V., J.Pou., and S.S.T. acknowledge support from Russian Science Foundation grant 20-12-00364 and the Academy of Finland grants 333112, 347003, 349144, and 349906. M.N. acknowledges support from NASA under award number 80GSFC21M0002. T.K. is supported by JSPS KAKENHI Grant Number JP19K03902. P.-O.P. acknowledges support from the High Energy National Programme (PNHE) of Centre national de la recherche scientifique (CNRS) and from the French space agency (CNES) as well as from the Barrande Fellowship Programme of the Czech and French governments. D.B., S.K., N.M., and R.S. acknowledge support from the European Research Council (ERC) under the European Union's Horizon 2020 research and innovation program under grant agreement no. 771282. V.Kr. thanks Vilho, Yrjö and Kalle Väisälä Foundation. P.T. and J.W. acknowledge funding from Bundesministerium für Wirtschaft und Klimaschutz under Deutsches Zentrum für Luft- und Raumfahrt grant 50 OR 1909. A.I. acknowledges support from the Royal Society. J.H. acknowledges the support of the Natural Sciences and Engineering Research Council of Canada (NSERC), funding reference number 5007110, and the Canadian Space Agency. S.G.J. and A.P.M. are supported in part by National Science Foundation grant AST-2108622, by NASA Fermi Guest Investigator grant 80NSSC21K1917, and by NASA Swift Guest Investigator grant 80NSSC22K0537. C.-Y.N. is supported by a General Research Fund of the Hong Kong Government under grant number HKU 17305419. P.Sl. acknowledges support from NASA Contract NAS8-03060. **Author contributions:** H.K., F.Mu., M.D., A.V., N.R.C., J.S., A.I., G.M., J.A.G., V.L., and J.Pou. participated in the planning of the observation campaign and the analysis and modeling of the data. M.N., T.K., J.Pod., J.R., and W.Z. contributed to the analysis or modeling of the data. A.V.B., V.Kr., S.V.B., M.K., T.S., D.B., S.K., N.M., and R.S. contributed to the optical polarimetric data. J.M.M. and P.D. contributed the Swift results; J.W. and P.T. the INTEGRAL results; and A.A.L., S.V.M., and A.N.S. the SRG/ART-XC results. S.B., F.C., N.D.L., L.L., A.Mar., T.M., N.O., A.R., P.-O.P, P.So., A.F.T., F.To., M.C.W., and S.Zh. contributed to the discussion of the results. F.Ma. and S.F. served as internal referees. All other authors contributed to the design and science case of the IXPE mission and to planning the observations used in this paper. All authors provided input and comments on the manuscript. **Competing interests:** The authors declare no competing interests. **Data and materials availability:** The May and June IXPE observations are available at https://heasarc.gsfc.nasa.gov/FTP/ixpe/data/obs/01/01002901/ and https://heasarc.gsfc.nasa.gov/FTP/ixpe/data/obs/01/01250101/, respectively. The NICER data are available at https://heasarc.gsfc.nasa.gov/docs/nicer/nicer_archive.html under ObsIDs 5100320101, 5100320102, 5100320103, 5100320104, 5100320105, 5100320106, and 5100320107. The NuSTAR data are available at https://heasarc.gsfc.nasa.gov/db-perl/W3Browse/w3table.pl?tablehead=name%3Dnumaster&Action=More+Options under ObsIDs 30702017002, 30702017004, and 30702017006. The SWIFT XRT data are available at https://heasarc.gsfc.nasa.gov/cgi-bin/W3Browse/swift.pl under ObsIDs 00034310009, 00034310010, 00034310011, 00034310012, 00034310013, and 00034310014. The extracted INTEGRAL ISGRI data are archived at Zenodo (*32*). The SRG ART-XC data are available at ftp://hea.iki.rssi.ru/public/SRG/ART-XC/data/Cygnus_X-1/. The MAXI light curves are available at http://maxi.riken.jp/star_data/J1958+352/J1958+352.html. The raw DIPol-2 and RoboPol data are archived at Zenodo (*33*, *34*). The KERRC code (*13*) is available at https://gitlab.com/krawcz/kerrc-x-ray-fitting-code.git. The MONK code (*35*) is available at https://projects.asu.cas.cz/zhang/monk. The ixpeobssim software is available at https://github.com/lucabaldini/ixpeobssim and documented at https://ixpeobssim.readthedocs.io. Our derived x-ray polarization measurements are listed in tables S1 and S2, and the optical polarization measurements are listed in table S4. The numerical results of our model fitting are listed in table S5. Our models of polarized emission in the truncated disk geometry are archived at Zenodo (*36*).

SUPPLEMENTARY MATERIALS

science.org/doi/10.1126/science.add5399
Materials and Methods
Figs. S1 to S12
Tables S1 to S5
References (*37*–*79*)

Submitted 18 June 2022; accepted 17 October 2022
Published online 3 November 2022
10.1126/science.add5399

Science

Polarized x-rays constrain the disk-jet geometry in the black hole x-ray binary Cygnus X-1

Henric KrawczynskiFabio MuleriMichal Dov#iakAlexandra VeledinaNicole Rodriguez CaveroJiri SvobodaAdam IngramGiorgio MattJavier A. GarciaVladislav LoktevMichela NegroJuri PoutanenTakao KitaguchiJakub PodgornýJohn RankinWenda ZhangAndrei BerdyuginSvetlana V. BerdyuginaStefano BianchiDmitry BlinovFiamma CapitanioNiccolò Di LallaPaul DraghisSergio FabianiMasato KagitaniVadim KravtsovSebastian KiehlmannLuca LatronicoAlexander A. LutovinovNikos MandarakasFrédéric MarinAndrea MarinucciJon M. MillerTsunefumi MizunoSergey V. MolkovNicola OmodeiPierre-Olivier PetrucciAjay RatheeshTakeshi SakanoiAndrei N. SemenaRaphael SkalidisPaolo SoffittaAllyn F. TennantPhillipp ThalhammerFrancesco TombesiMartin C. WeisskopfJoern WilmsSixuan ZhangIván AgudoLucio A. AntonelliMatteo BachettiLuca BaldiniWayne H. BaumgartnerRonaldo BellazziniStephen D. BongiornoRaffaella BoninoAlessandro BrezNiccolò BucciantiniSimone CastellanoElisabetta CavazzutiStefano CipriniEnrico CostaAlessandra De RosaEttore Del MonteLaura Di GesuAlessandro Di MarcoImmacolata DonnarummaVictor DoroshenkoSteven R. EhlertTeruaki EnotoYuri EvangelistaRiccardo FerrazzoliShuichi GunjiKiyoshi HayashidaJeremy HeylWataru IwakiriSvetlana G. JorstadVladimir KarasJeffery J. KolodziejczakFabio La MonacaIoannis LiodakisSimone MalderaAlberto ManfredaAlan P. MarscherHerman L. MarshallIkuyuki MitsuishiChi-Yung NgStephen L. O’DellChiara OppedisanoAlessandro PapittoGeorge G. PavlovAbel L. PeirsonMatteo PerriMelissa Pesce-RollinsMaura PiliaAndrea PossentiSimonetta PuccettiBrian D. RamseyRoger W. RomaniCarmelo SgròPatrick SlaneGloria SpandreToru TamagawaFabrizio TavecchioRoberto TavernaYuzuru TawaraNicholas E. ThomasAlessio TroisSergey TsygankovRoberto TurollaJacco VinkKinwah WuFei XieSilvia Zane

Science, 378 (6620), • DOI: 10.1126/science.add5399

x-ray polarization of Cygnus X-1
A black hole in a binary system can rip material off of its companion star, which heats up and forms an accretion disk. The disc emits light in the optical and x-ray bands, forming an x-ray binary (XRB) system. Some XRBs also launch a jet of fast-moving material that is visible at radio wavelengths. Krawczynski *et al*. observed the x-ray polarization of Cygnus X-1, a black hole XRB with a radio jet. By comparing the measured polarization properties with several competing XRB models, they eliminated some hypothesized geometries and determined that the x-ray–emitting region extends parallel to the accretion disc. —KTS